Articles

Silver Antimonates with Pyrochlore-like Structure Prepared by Thermal Treatment of Silver Proton-Exchanged Antimonic Acid: Formation Process and Structural Characterization

Aldo J. G. Zarbin,[†] Oswaldo L. Alves,[†] J. Manuel Amarilla,[‡] Rosa M. Rojas,[‡] and José M. Rojo*[,‡]

Laboratório de Química do Estado Solido, Instituto de Química, UNICAMP, CP 6154, 13081 Campinas, SP, Brazil, and Instituto Ciencia de Materiales de Madrid, Consejo Superior de Investigaciones Científicas, Cantoblanco, 28049 Madrid, Spain

Received June 1, 1998. Revised Manuscript Received January 20, 1999

Silver proton-exchanged antimonic acids, with pyrochlore-type structure and composition of $H_{2-x}Ag_xSb_2O_6 \cdot nH_2O$, ($0 < x < 2$) have been obtained, and they have been used as precursors for preparing silver antimonates. The ionic conductivity of the silver proton-exchanged samples as prepared is dominated by proton motion, which is clearly affected by the water content. The formation reaction of silver antimonates has been followed by thermal analysis, mass spectrometry, X-ray diffraction, etc. Four regions can be distinguished: (i) from room temperature to 400 °C, weakly bonded water and protons are removed as water; (ii) from 400 to 600 °C, oxygen is removed from the pyrochlore framework leading to reduction of some Sb^{5+} to Sb^{3+}; (iii) from 600 to 950 °C, thermally stable silver antimonates with pyrochlore-like structure are formed with the amount of Sb^{3+} decreasing on increasing the silver content; and (iv) above 950 °C, the silver antimonates decompose giving β-Sb_2O_4, which sublimates, and metallic silver. Crystal structure of the silver antimonates has been analyzed by X-ray diffraction. According to the Rietveld refinement, Ag^+ and Sb^{3+} are placed in the channels of the pyrochlore-like structure.

Introduction

Antimonic acids with a variety of structures (ilmenite, cubic $KSbO_3$, pyrochlore, amorphous) exhibit high protonic conductivities[1−6] and negligible electronic conductivity.[7] In the case of the pyrochlore-type structure, the characteristic structural feature is a $[Sb_2O_6^{2-}]_n$ three-dimensional framework built up from infinite chains of corner-shared SbO_6 octahedra. Water molecules and acidic protons occupy the interstitial cavities within the framework; the cavities being interconnected[1]. The electrical conductivity of the antimonic acid has been investigated by ac and dc conductivity techniques under different water vapor pressures.[8−10] From these investigations, it has been concluded that the material is a protonic conductor whose ionic conductivity at room temperature ranges from 10^{-4} to 10^{-3} S cm^{-1} depending on the relative humidity. The overall conductivity of pellets seems to be affected by two contributions: grain-interior and grain-boundary conductivity. The first arises from the fact that the material shows a framework with channels in which hydrated protons can move easily. The second is due to the protonic motion through borders of neighboring particles. The presence of the grain-interior conductivity marks a difference with other protonic conductors such as $ZrO_2 \cdot nH_2O$ and $SnO_2 \cdot nH_2O$, classified as "particle hydrates", where conductivity is only due to the second effect, i.e., motion of protons in an external aqueous region linking together the crystalline particles.[1]

[†] Laboratório de Química do Estado Solido.
[‡] Instituto Ciencia de Materiales de Madrid.

(1) England, W. A.; Cross, M. G.; Hamnett, A; Wiseman, P. J.; Goodenough, J. B. *Solid State Ionics* **1980**, *1*, 231.
(2) Chowdhry, U.; Barkley, J. R.; English, A. D.; Sleight, A. W. *Mater. Res. Bull.* **1982**, *17*, 917.
(3) England, W. A.; Slade, R. C. T. *Solid State Commun.* **1980**, *33*, 997.
(4) Dzimitrowicz, D. J.; Goodenough, J. B.; Wiseman, P. J. *Mater. Res. Bull.* **1982**, *17*, 971.
(5) Forano, C.; Besse, J. P.; Battut, J. P.; Dupuis, J.; Hajjimohamad, A. *Solid State Ionics* **1989**, *34*, 7.
(6) Turrillas, X.; Delabouglise, G.; Joubert, J. G.; Fournier, T.; Muller, J. *Solid State Ionics* **1985**, *17*, 169.
(7) Matiyasevich, A. M.; Karaseva, T. A. *Russ. J. Phys. Chem.* **1989**, *63*, 594.
(8) Ozawa, Y.; Miura, N.; Yamazoe, M.; Seiyama, T. *Chem. Lett.* **1983**, 1569.
(9) Slade, R. C. T.; Hall, G. P.; Skou, E. *Solid State Ionics* **1989**, *35*, 29.
(10) Bajars, G. E.; Linhardt, P.; Breiter, M. W. *Electrochim. Acta* **1990**, *35*, 1031.

10.1021/cm9803915 CCC: $18.00
Published on Web 06/04/1999

The antimonic acid with pyrochlore-type structure shows proton-exchange reactions with alkali metal ions, alkaline earth metal ions, and other ions such as Ni^{2+}, Mn^{2+}, Cd^{2+}, Fe^{3+}, etc.[11−15] This property has also been used for preparing precursors that in a subsequent thermal treatment yield materials usable as catalysts ($FeSbO_4$) and semiconductors ($Cd_2Sb_2O_{7-x}$).[16,17] Regarding the silver proton-exchange reaction, an exchange capacity of ca. 5 mequiv of Ag^+/g has been reported by different authors,[11,14,18] although some uncertainties about the antimonic acid used still remains. For example, the acid used was called polyantimonic acid, hydrated antimonic pentoxide, crystalline antimonic acid, etc. and represented by different formulas. In the case of the so-called crystalline antimonic acid, it has been reported that the lattice parameter decreases upon exchange with Ag^+ and, as a result, formation of a solid solution has been proposed.[18] The electrical properties of $AgSbO_3$ and other pyrochlore-like compounds have been studied by different authors.[19−24] However, several aspects such as the dependence of the ionic conductivity on the exchange ratio and the thermal transformations of the exchanged materials are still unknown.

The aim of this work is to study the formation of silver antimonates by using silver proton-exchanged compounds derived from the antimonic acid as precursors. The precursors are prepared by an ion exchange reaction, and their ionic conductivity is studied. Thermal treatment of the precursors leads to the corresponding silver antimonates. The crystal structure is investigated by Rietveld refinement of their X-ray diffraction data, and the distribution of Sb^{3+} and Ag^+ in the pyrochlore network is analyzed.

Experimental Section

Antimonic acid with pyrochlore structure was synthesized following a procedure described elsewhere.[25] A total of 12 g of Sb_2O_3 (Merck) was oxidized with 120 mL of H_2O_2 (Merck) with the suspension being stirred at 65 °C for 30 h. Once the antimonic acid was obtained, it was washed with deionized water and centrifuged; finally, it was dried at 40 °C under low pressure and air-stored. Water content of the antimonic acid was deduced from the thermogravimetric curve. The weight loss observed between room temperature and 700 °C, at which Sb_6O_{13} is formed as a single compound, allowed us to determine the water content of the starting antimonic acid.

Silver proton-exchanged compounds of the general formula $H_{2-x}Ag_xSb_2O_6 \cdot nH_2O$ ($0 < x < 2$) were prepared by ion exchange reaction of the starting antimonic acid ($H_2Sb_2O_6 \cdot 1.5H_2O$) with an $AgNO_3$ solution (0.04 M) in the adequate stoichiometry. The suspension was stirred at room temperature for 24 h. Then the solid was separated, washed several times, and dried in the same way as for the antimonic acid. To prepare the fully exchanged sample, $x = 2$, an excess of $AgNO_3$ solution was added; however, the exchange reaction did not proceed further than $x = 1.7$. The degree of exchange was deduced from the quantitative determination of silver (Volhard's method) in the $AgNO_3$ solution after the exchange reaction and by measuring the concentration of the liberated protons (pH measurement). In the case of samples at $x = 0.5$, 1, and 1.5, no silver was detected in the mother solution after the exchange reaction. The silver content in the solid samples was also determined by atomic absorption analysis of the solution obtained by alkaline melting (sodium carbonate/sodium thiosulfate) of the samples. The antimony and silver content in the starting silver-exchanged samples and in the silver antimonates obtained by heating at 700 °C was analyzed by X-ray energy-dispersive spectroscopy (XEDS) in a JEOL 2000 FX electron microscope. The samples were previously ground in acetone and dispersed on copper grids coated with holey-carbon support film. Several crystals of each composition were analyzed.

X-ray diffraction patterns were recorded at room temperature on a Siemens D501 diffractometer with Cu Kα radiation. The patterns were scanned at 0.02° (2θ) step scan, and 1 s per step counting time in the range $10° \leq 2\theta \leq 80°$. Cell parameters were refined by using the program CELREF.[26] For the Rietveld refinement, patterns of the silver antimonates were recorded at 0.02(2θ) step scan between $10° \leq 2\theta \leq 110°$ and 10 s per step counting time. The refinement was undertaken with the program FULLPROF[27].

Differential thermal analysis (DTA) and thermogravimetric (TG) curves were simultaneously recorded on a Seiko 320 U instrument. A 10−15 mg batch of each sample was heated at 5 °C min^{-1} in N_2 or Ar flow and in still air; α-Al_2O_3 was used as reference material. Simultaneous qualitative analysis of the gases evolved during the thermal treatments (EGA) was carried out with a ThermoStar mass spectrometer, which used Ar as the carrier.

Impedance measurements were carried out in an impedance/gain-phase analyzer (Solartron 1260). The frequency range used was 5 Hz to 5 MHz. Pellets of 12 mm diameter and ca. 1 mm thickness were prepared by pressing the powder samples at 150 MPa. Gold electrodes were deposited on the two faces of the pellets by vacuum evaporation; then, the pellets were rehydrated at the atmosphere and air-stored. The impedance measurements were done in the range 20−220 °C, while the pellet was at a steady temperature under nitrogen flow.

Results

Thermal and Chemical Analyses. The TG curves for the four silver proton-exchanged samples are shown in Figure 1a. The TG curve recorded for the antimonic acid ($x = 0$) is also shown for comparison. Three well-defined weight losses and one plateau are observed. The first weight loss region ranges from room temperature to 400 °C, the second one ranges from 400 to 600 °C, the plateau goes from 600 to 950 °C, and the third weight loss takes place above 950 °C. The thermogravimetric curve recorded for the antimonic acid shows a fourth weight loss between 850 and 900 °C. It has been associated with the formation of β-Sb_2O_4, which subli-

(11) Lefebvre, J.; Gaymard, F. *C. R. Acad. Sci. Paris* **1965**, *260*, 6911.
(12) Abe, M.; Itoh, T. *Bull. Chem. Soc. Jpn*. **1968**, *41*, 33.
(13) Abe, M.; Itoh, T. *Bull. Chem. Soc. Jpn*. **1968**, *41*, 2366.
(14) Baetsle, L. H.; Huys, D. *J. Inorg. Nucl. Chem*. **1968**, *30*, 639.
(15) Abe, M.; Itoh, T. *J. Inorg. Nucl. Chem*. **1980**, *42*, 1641.
(16) Zarbin, A. J. G.; Alves, O. L. *J. Mater. Sci. Lett*. **1994**, *13*, 607.
(17) Zarbin, A. J. G.; Alves, O. L. *J. Mater. Chem*. **1994**, *4*, 389.
(18) Abe, M.; Akimoto, M. *Bull. Chem. Soc. Jpn*. **1980**, *53*, 121.
(19) Watelet, H.; Besse, J. P.; Baud, G.; Chevalier, R. *Mater. Res. Bull*. **1980**, *15*, 875.
(20) Matsumoto, Y.; Funaki, K.; Hombo, J.; Ogawa, Y. *J. Solid State Chem*. **1992**, *99*, 336.
(21) Yasukawa, M.; Hosono, H.; Ueda, N.; Kawazoe, H. *Jpn. J. Appl. Phys*. **1995**, *34*, 281.
(22) Wiggers, H.; Simon, U.; Schön, G. *Solid State Ionics* **1998**, *107*, 111.
(23) Isasi, J.; Lopez, M. L.; Veiga, M. L.; Pico, C. *Solid State Ionics* **1996**, *89*, 321.
(24) Tuller, H. L. *Solid State Ionics* **1997**, *94*, 63.
(25) Ozawa, Y.; Miura, N.; Yamazoe, N.; Seiyama T. *Chem. Lett*. **1982**, 1741.
(26) Raugier, J.; Filhol, A. CELREF, I.L.L., Grenoble, France, unpublished, PC version 1991.
(27) Rodriguez-Carvajal, J. FULLPROF, I.L.L., Grenoble, France, unpublished, PC version 1995.

Table 1. Chemical, XEDS, and TG Analyses for the Silver Proton-Exchanged Precursors, and XEDS Analysis for the Silver Antimonates[a]

chemical analysis for couples at rt		XEDS analysis		weight loss (%)			composition of compd	
Ag/Sb ratio	Ag (wt %)	Ag/Sb ratio for samples at rt	Ag/Sb ratio for samples at 700 °C	region I (rt−400 °C)	region II (400°−600 °C)	starting composition	formed at 700 °C	Sb^{3+}/Sb_{total} (%)
				12.4	3.0	$H_2Sb_2O_6{\cdot}1.5H_2O$	$Sb_2O_{4.31}$	33.3
0.25	12.7	0.25	0.24	10	1.6	$Ag_{0.5}H_{1.5}Sb_2O_6{\cdot}1.5H_2O$	$Ag_{0.5}Sb_2O_{4.83}$	21
0.5	23	0.47	0.46	6.03	1.1	$AgHSb_2O_6{\cdot}1H_2O$	$AgSb_2O_{5.18}$	16
0.75	30.5	0.74	0.72	4.33	0.71	$Ag_{1.5}H_{0.5}Sb_2O_6{\cdot}1H_2O$	$Ag_{1.5}Sb_2O_{5.52}$	11.5
0.82	34	0.84	0.84	2.54	0.24	$Ag_{1.7}H_{0.3}Sb_2O_6{\cdot}0.5H_2O$	$Ag_{1.7}Sb_2O_{5.77}$	4

[a] Chemical formulas deduced for both types of compounds. Calculated Sb^{3+}/Sb_{total} for the silver antimonates is included. All antimony is Sb^{5+} in the samples as prepared. rt, room temperature.

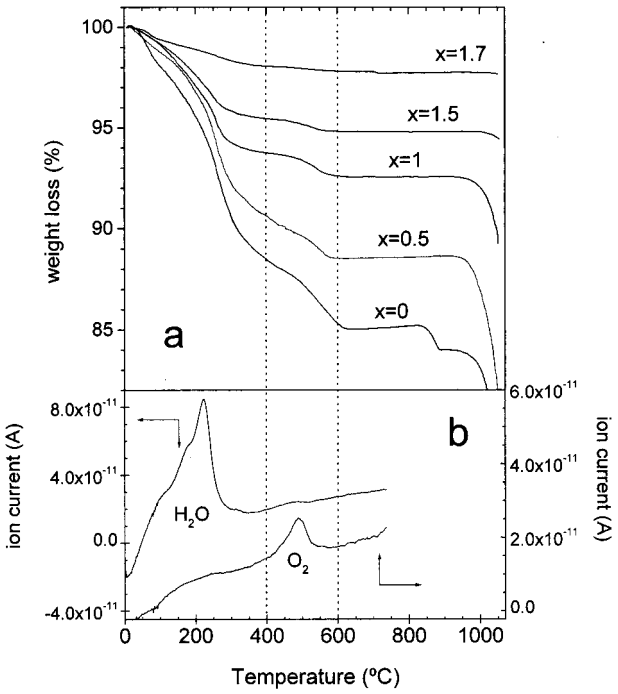

Figure 1. (a) TG curves recorded for the $H_{2-x}Ag_xSb_2O_6{\cdot}nH_2O$ ($x = 0$, 0.5, 1, 1.5, and 1.7) precursors. (b) Mass spectrometry analysis of the gases evolved during the thermal treatment of the sample at $x = 1$.

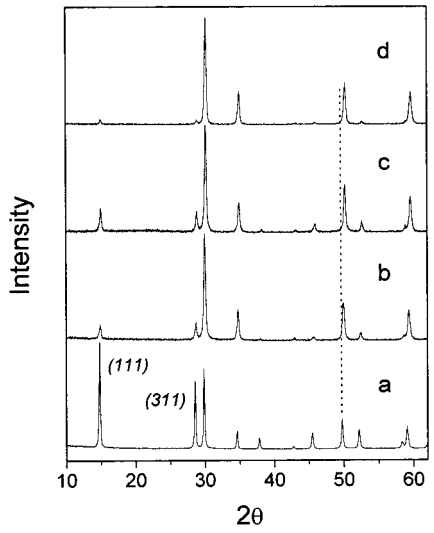

Figure 2. X-ray powder diffraction patterns recorded at room temperature for the silver proton-exchanged samples as prepared: $x = 0$ (a), $x = 1$ (b), and after heating at 700 °C: $x = 0$ (c), $x = 1$ (d).

mates at about 1000 °C.[28] Gases evolved during the thermal treatment of the silver-exchanged samples were simultaneously analyzed by mass spectrometry. In Figure 1b, the evolving gases vs temperature are shown for the sample at $x = 1$. Water vapor and oxygen gas were released in the temperature ranges of 20−300 and 400−550 °C, respectively, which are within the intervals at which the first and second weight losses had been observed in the TG curves. A possible contamination of the analysis probe as a consequence of some sublimation prevented us for analyzing the gases evolved at $T > 800$ °C.

Silver and antimony contents for the silver proton-exchanged samples as prepared and after heating at 700 °C were determined according to the chemical and XEDS analyses described in the Experimental Section. Results of the analyses together with the weight loss found in the temperature ranges of room temperature−400 °C and 400−600 °C are outlined in columns 1−6 in Table 1.

X-ray Powder Diffraction. The X-ray powder diffraction patterns of the starting antimonic acid ($x = 0$) and of one of the silver proton-exchanged samples ($x = 1$) are shown in Figure 2, panels a and b, respectively. These patterns, which are typical for all compositions, can be fully indexed on the basis of a pyrochlore-type structure (space group $Fd\bar{3}m$). On comparing the patterns, it is observed that on increasing the Ag^+ content (i) the reflections shift toward higher 2θ angles and (ii) the intensity of maxima with $(h+k+l)$ odd number, such as the (111) and (311) marked in the figure, progressively decreases. The X-ray diffraction patterns recorded for those samples once they had been heated to 700 °C are also shown in Figure 2, panels c and d. The patterns are also consistent with the pyrochlore-type structure, although some differences with those of the starting samples are observed. The X-ray diffraction maxima of the heated samples are shifted again toward higher 2θ angles and the intensity of the $(h+k+l)$ odd reflections is even lower.

In Figure 3, values of the lattice parameter vs Ag/Sb ratio for the samples as prepared (closed squares) and after heating to 700 °C (closed circles) are plotted. In both cases, a solid solution is formed in the whole composition range explored. In this figure, the lattice parameters reported by other authors for the starting silver-exchanged compounds[18] and for silver anti-

(28) Stewart, D. J.; Knop, O.; Ayasse, C.; Woodhams, F. W. D. *Can. J. Chem.* **1972**, *50*, 690.

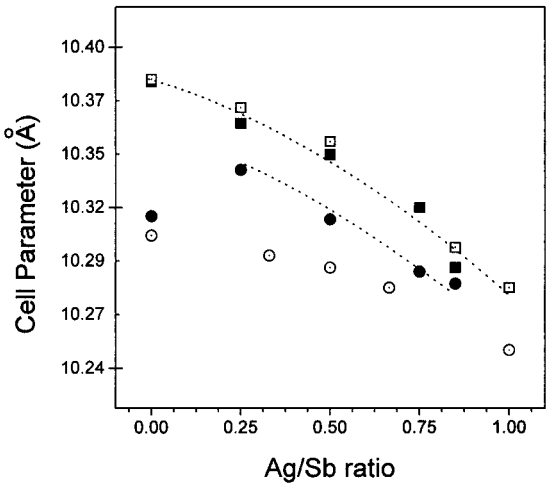

Figure 3. Cell parameter vs Ag/Sb ratio for the silver proton-exchanged precursors (closed squares) and for the silver antimonates formed at 700 °C (closed circles). Data reported for the former compounds (open squares, ref 18) and for the latter ones prepared by a ceramic procedure (open circles, ref 28) are also included.

monates prepared by a ceramic procedure[29] have also been included for comparison. It can be seen that they fairly agree, within experimental error, with our data.

Ionic Conductivity. The impedance plots (imaginary vs real part) recorded at two temperatures for a pellet of the sample at $x = 0.5$ are shown in Figure 4. These data are typical of all compositions. At 20 °C, only an inclined spike and a portion of an arc are observed; however, at 200 °C two arcs, one of them at high frequency and the other at low frequency, are clearly observed. The capacitance associated with the high-frequency and low-frequency arcs are in the ranges of 5−10 pF and 10−70 nF, respectively. The spike shows a capacitance, given from the ideal relation $Z'' = 1/\omega C$, of 5−15 μF. From these data, it may be concluded that the samples are ionic conductors; the high-frequency arc is ascribed to motion of the ions within the grains, i.e., in the structure (grain-interior response); and the low-frequency arc is due to motion of the ions through the boundaries of neighboring grains (grain-boundary response). The overall resistance of the pellet can be determined from the intercept of either the spike or the low-frequency end of the low-frequency arc on the real Z' axis.[30] From the intercept of the low-frequency end of the high-frequency arc on the real axis, the grain-interior resistance can also be determined. In some particular cases, only one arc and the spike were observed in the impedance plots. For example, the impedance plots of pellets of pure antimonic acid only showed one arc in which the grain-interior and grain-boundary responses were overlapped. We could not separate the contribution due to the two responses under the experimental conditions adopted.

Discussion

The progressive silver proton-exchange in antimonic acid yields compounds that maintain the pyrochlore framework. To make the discussion of the thermal transformation undergone by the precursors easier, four temperature regions have been considered.

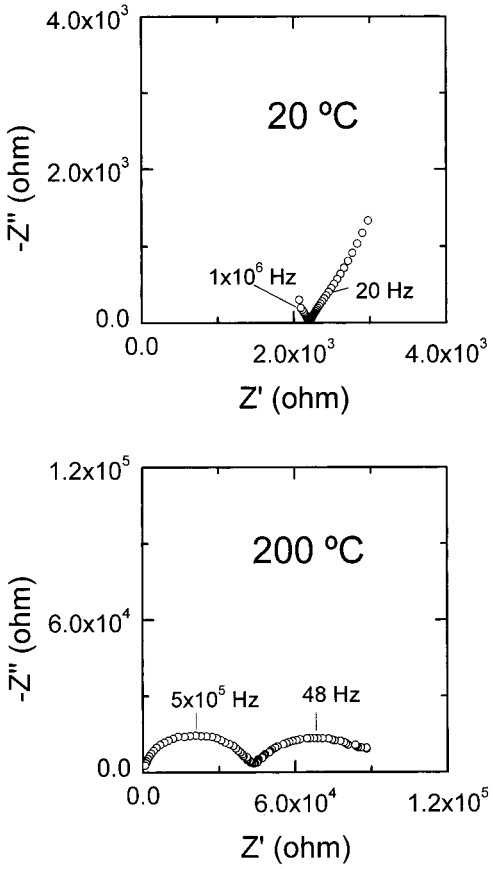

Figure 4. Impedance plots (imaginary vs real part) obtained at two temperatures for the sample at $x = 0.5$.

Region I: from Room Temperature to 400 °C. In this temperature interval, the TG curves show a continuous weight loss with several change of slope. The weight loss is due to release of water according to mass spectrometry. The mass spectrum (Figure 1b) shows several shoulders at the lower temperature side of the H_2O peak, indicating different stages for the water removal. However, attempts for quantifying the more weakly bonded water and the structural water were unsuccessful. Simultaneously recorded DTA curves (not shown in Figure 1) did not provide further information.

Conductivity measurements carried out on pellets of different compositions in the 20−220 °C interval also indicate the presence of several types of water. The overall ionic conductivity of the pellets ($x = 0$, 0.5, 1, and 1.7) against temperature is shown in an usual Arrhenius plot (Figure 5a). In all cases data were obtained in a heating run at steady temperatures. Three temperature ranges can be distinguished: one range between room temperature and 100 °C, another one between 100 and 160 °C, and another range between 160 and 220 °C. In the first range, a decrease in conductivity for all samples is observed. At this stage the more weakly bounded water is removed, and the decrease in conductivity can be explained by a decrease in mobility of the ionic carriers. The concentration of charge carriers should not be affected in this temperature range. In the second range, although dehydration

(29) Stewart, D. J.; Knop, O. C. *Can. J. Chem.* **1970**, *48*, 690.
(30) Macdonald, J. R. *Impedance Spectroscopy, Emphasizing Solid Materials and Systems*; New York, Wiley: 1987.

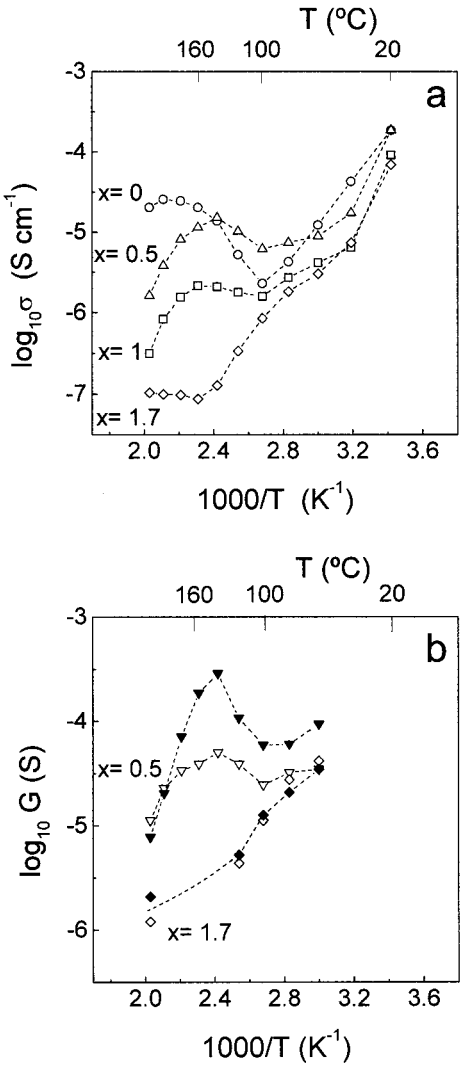

Figure 5. (a) Overall ionic conductivity vs inverse temperature for the samples at $x = 0$, 0.5, 1, and 1.7. (b) Conductance of the grain-interior (open symbols) and grain-boundary (closed symbols) response vs inverse temperature for the samples at $x = 0.5$ and 1.7.

continues, different trends for the conductivity are found. The conductivity increases for the samples at $x = 0$ and 0.5, remains constant for the sample $x = 1$, and decreases for the sample $x = 1.7$. We have no explanation for the different trends observed; however, the ionic conductivity measured depends on proton content, showing higher values for higher proton contents. This result points out that, despite the presence of Ag^+ ions, the ionic conductivity is dominated by the motion of protons. In the third range, above 160 °C, a decrease in conductivity is observed for the proton-enriched samples. This fact suggests that the proton motion mechanism does not work any more due to the absence of water in the tunnels. The ionic conductivity measured for the sample at $x = 1.7$ in the third temperature range is close to the values reported for $AgSbO_3$ in which the charge carriers are Ag^+ ions.[22] The absence of linear dependencies in the three analyzed temperature ranges prevented us from determining the activation energy associated with the ionic motion.

To ascertain whether the behavior observed for the overall conductivity against inverse temperature is also followed by the grain-interior conductivity, the conductance due to the grain-interior and grain-boundary responses is plotted in the Arrhenius formalism (Figure 5b) for the samples at $x = 0.5$ and 1.7. We have chosen these compositions because their impedance plots showed well-resolved grain-interior and grain-boundary arcs. Conductance, $G = 1/R$, was used instead of conductivity because of the difficulty for estimating the surface area of the grain boundaries. It is observed (Figure 5b) that the grain-interior and grain-boundary conductance follow the same trend as for the overall conductivity, and the two conductances are quite similar. Therefore, the overall conductivity is a parameter representative of the grain-interior response and, hence, of the silver proton-exchanged samples.

Region II: from 400 to 600 °C. According to the mass spectrometry data (Figure 1b), the weight loss undergone by the silver-exchanged compounds in this temperature interval is unambiguously ascribed to release of oxygen. Release of water was not detected. Therefore, the samples must be reduced with transformation of some Sb^{5+} into Sb^{3+}. The reduction reaction in pure antimonic acid was formerly proposed by Stewart et al.[28] and later confirmed by isothermal volumetric analysis of oxygen.[31]

Having in mind that the thermal treatment of the samples through regions I and II produces removal of water and oxygen, reactions taking place from room temperature to 600 °C can be expressed as follows:

$$H_{2-x}Ag_xSb_2O_6{\cdot}nH_2O \xrightarrow[\text{region I}]{\text{rt} - 400\ ^\circ\text{C}} Ag_xSb_2O_{6-(2-x)/2} + nH_2O\uparrow + (2-x)/2H_2O\uparrow$$

$$Ag_xSb_2O_{6-(2-x)/2} \xrightarrow[\text{region II}]{400-600\ ^\circ\text{C}} Ag_xSb_2O_{6-y-(2-x)/2} + y/2O_2\uparrow$$

Taking into account (i) the overall weight loss up to 700 °C, ascribed to the removal of water and oxygen, and (ii) the values of x deduced from chemical analysis and XEDS, the chemical formulas for both the starting and the compounds formed at 700 °C have been determined (Table 1). The Ag/Sb ratio, deduced from XEDS analysis, is the same for either the starting samples and its derivatives. It points out that heating to 700 °C does not produce any variation in the silver and antimony content. The percentage of Sb^{3+} deduced from the chemical formulas of silver antimonates formed at 700 °C is also included in the latest column of Table 1. This percentage decreases for increasing silver content, indicating a higher stability against reduction for the silver-enriched samples.

Region III: from 600 to 900 °C. In this temperature range, all the TG curves show a plateau indicating that thermally stable compounds are formed. The samples obtained at 700 °C show X-ray patterns analogous to those recorded for the starting materials, indicating that the compounds are single-phase pyrochlore-type. The lattice parameter of these samples (closed circles in Figure 3) is lower than that found for the precursors and fairly agrees with values reported for silver anti-

(31) Klestchov, D.; Burmistrov, V.; Sheinkman, A.; Pletnev, R. *J. Solid State Chem.* **1991**, *94*, 220.

Table 2. Crystallographic Data, Bond Distances, and Structural Formulas Deduced from the Rietveld Refinement for Silver Antimonates Formed at 700 °C

	$Ag_{0.5}Sb_2O_{4.83}$	$AgSb_2O_{5.18}$	$Ag_{1.5}Sb_2O_{5.52}$	$Ag_{1.7}Sb_2O_{5.77}$
space group	$Fd\bar{3}m$	$Fd\bar{3}m$	$Fd\bar{3}m$	$Fd\bar{3}m$
a (Å)	10.3388(5)	10.3178(6)	10.2892(5)	10.2820(1)
cell vol (Å^3)	1105.1	1098.5	1089.3	1087.0
Z	8	8	8	8
2θ range, time/step	10−110°, 10 s	10−110°, 10 s	10−98°, 10 s	10−98°, 10 s
no. of hkl	96	95	78	78
refinable atomic parameter	11	11	11	11
reliability factors	$R_p = 12.1$, $R_{wp} = 16.2$ $\chi^2 = 4.31$, $R_{Bragg} = 11.5$	$R_p = 11.7$, $R_{wp} = 16.3$ $\chi^2 = 4.5$, $R_{Bragg} = 9.5$	$R_p = 12.2$, $R_{wp} = 17.8$ $\chi^2 = 5.6$, $R_{Bragg} = 8.6$	$R_p = 11.8$, $R_{wp} = 16.5$ $\chi^2 = 5.3$, $R_{Bragg} = 10.5$
x(O) (48f)	0.336(2)	0.354(3)	0.360(5)	0.355(4)
occ (Sb^{3+}) (16d)	0.250(2)	0.180(3)	0.137(9)	0.035(3)
occ (Ag^+) (16d)	0.315	0.595	0.845	0.885
occ (O′) (8a)	0.1	0.13	0.25	
$B_{overall}$	0.74(2)	0.90(2)	0.72(3)	0.88(3)
		Bond Distances		
d(Sb^{5+}−O) (Å)	2.036(9)	2.12(2)	2.14(3)	2.11(2)
d(Sb^{3+}, Ag^+−O) (Å)	2.487(8)	2.36(2)	2.32(3)	2.35(2)
d(Sb^{3+}, Ag^+−O′) (Å)	2.238	2.234	2.228	
d(O−O) (Å)	3.10(2)	3.34(2)	3.41(5)	3.34(4)
	2.644(3)	2.597(3)	2.582(5)	2.587(5)
d(O−O′) (Å)	2.98(1)	2.80(3)	2.73(6)	
	3.677(2)	3.654(2)	3.641(2)	
structural formulas	$[Ag^+_{0.63}Sb^{3+}_{0.50}]_{16d}[Sb^{5+}_2]_{16c}$-$[O_6]_{48f}[O_{0.1}]_{8a}$	$[Ag^+_{1.19}Sb^{3+}_{0.36}]_{16d}[Sb^{5+}_2]_{16c}$-$[O_6]_{48f}[O'_{0.13}]_{8a}$	$[Ag^+_{1.69}Sb^{3+}_{0.27}]_{16d}[Sb^{5+}_2]_{16c}$-$[O_6]_{48f}[O'_{0.25}]_{8a}$	$[Ag^+_{1.77}Sb^{3+}_{0.07}]_{16d}[Sb^{5+}_2]_{16c}$-$[O_6]_{48f}$

monates obtained by a ceramic procedure[29] (open circles in Figure 3). The variation of the lattice parameter of the formed samples on increasing the silver content (Figure 3) suggests that we are dealing, in the whole composition range, with a solid solution. Therefore, thermal treatment of the starting $H_{2-x}Ag_xSb_2O_6 \cdot nH_2O$ ($0 < x < 2$) samples constitutes a straightforward procedure for the synthesis of silver antimonates with different chemical composition and pyrochlore-type structure.

To investigate the cation distribution in silver antimonates, the structure of each composition was investigated by Rietveld refinement of the powder X-ray diffraction patterns. The structural refinement was carried out on the basis of a framework with the pyrochlore-type structure (space group $Fd\bar{3}m$). The pyrochlore structure can be considered as built up of two interpenetrating A_2O' and B_2O_6 arrays. The latter B_2O_6 framework is necessary for the stability of the structure. The small B (≈0.6 Å ionic radius) cations are in an octahedral oxygen environment,[32] the octahedra forming a framework with interconnected channels in which the A and O′ atoms are located. The anion coordination about each large A cation (≈1 Å ionic radius) is a deformed cube or a puckered hexagonal bypiramid. It is worth mentioning that the pyrochlore structure $A_2B_2O_6O'$ tolerates vacancies at the A and O′ sites giving defect pyrochlores.[32,33]

Having in mind the similarity (position and intensity of the peaks) between the X-ray patterns of the silver antimonates and that of the Sb_6O_{13}, the crystal structure refinement was carried out, in all cases, on the basis of the structural model proposed by Stewart et al.[28] for $Sb_6O_{13}(Sb_2O_{4.33})$, which is obtained by heating antimonic acid between 650 and 850 °C. In Sb_6O_{13}, the arrangement that best accounts for the observed intensities is as follows: $[Sb^{3+}]_{16d}[Sb_2{}^{5+}]_{16c}[O_6]_{48f}[O']_{8a}$. The presence of Sb^{3+} in this oxide was undoubtedly confirmed by Mössbauer spectroscopy.[28] In our silver antimonates, the Sb^{3+} was placed at the 16d sites. Having in mind the ionic radius of the silver ion ($^{VIII}Ag^+ = 1.28$ Å),[34] it was also placed at the 16d sites of the $Fd\bar{3}m$ space group. In some other antimonates with monovalent[35,36] or divalent[37] cations, the large A cations are shifted from the 16d position, being situated at the 96g and/or 32e sites of the $Fd\bar{3}m$ group. Attempts to fit our patterns on the basis of these structural models were unsuccessful, leading to unacceptable reliability factors. The Rietveld refinement for each composition involved the zero point, the scale factor, the lattice constant, the profile parameters, the background parameter, and the appropriate position parameter x for the oxygen atom at the 48f site. The occupancy of the 16d site by Ag^+ for each composition was fixed according to the chemical and XEDS analysis data. In the final refinement, the occupancy of the Sb^{3+} was refined until the best fit was reached. The observed, calculated, and difference X-ray diffraction profiles for the sample at $x = 1.0$ is shown in Figure 6. Crystallographic data and structural formulation obtained for each composition are outlined in Table 2. The value of the coordinate x for the oxygen atoms at 48f is between 0.3125, which leads to a regular octahedral arrangement around the B cations at 16c, and 0.375, which gives a regular cube around the A cations.[32] The x value determined for the silver antimonates (Table 2) indicates that the coordination polyhedron around Sb^{5+} is a trigonal antiprism. It is worth mentioning that the content of Sb^{3+} determined from the Rietveld refinement fairly agrees with that deduced

(32) Subramanian, M. A.; Aravamudan, G.; Subba Rao, G. V. *Progr. Solid State Chem.* **1983**, *15*, 55.
(33) Hyde, B. G.; Andersson, S. *Inorganic Crystal Structures*; John Wiley and Sons: New York, 1989; p 344.
(34) Shannon, R. D. *Acta Crystallogr.* **1976**, *A32*, 751.
(35) Piffard, Y.; Dion, M.; Tournoux, M. *Acta Crystallogr.* **1978**, *B34*, 366.
(36) Piffard, Y.; Tournoux, M. *Acta Crystallogr.* **1979**, *B35*, 1450.
(37) Zouad, S.; Jeanjean, J.; Loos-Neskovic, C.; Fedoroff, M. *J. Solid State Chem.* **1992**, *98*, 1.

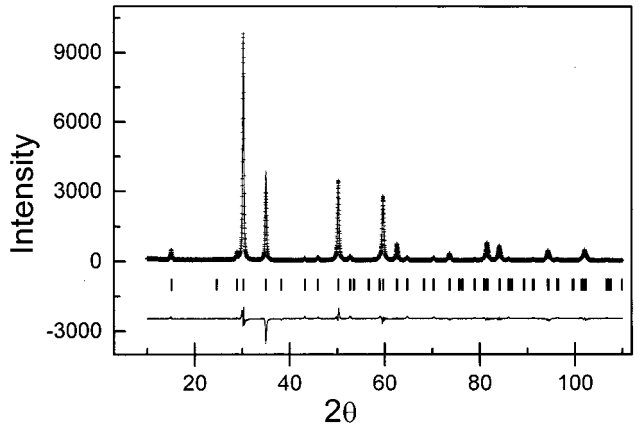

Figure 6. Calculated (−), experimental (+), and difference X-ray diffraction profiles for the $AgSb_2O_{5.18}$ (silver antimonate). The vertical lines below the profiles mark the position of all possible Bragg reflections.

from the chemical composition. Since Ag^+ occupies the same crystallographic site as Sb^{3+}, this position is less available for Sb^{3+} as the silver content increases. This fact would account for the decreasingly reduction undergone by the silver-enriched samples. The metal−oxygen and oxygen−oxygen distances are within the values reported for Sb-containing pyrochlores.[32,35−37]

Region IV: from 950 to 1050 °C. Above 950 °C the silver antimonates formed in region III undergo a continuous weight loss, which is particularly significant for the compounds having low silver content. In the case of the pure antimonic acid and between 850° and 900 °C (Figure 1a), there is another well-defined step that has been ascribed to removal of oxygen with the formation of β-Sb_2O_4.[28,31] It sublimates at $T > 1000$ °C giving rise to the weight loss observed above this temperature. For the silver antimonates, this intermediate stage is not observed, and only from 950 to 1050 °C is a continuous weight loss detected. The XEDS analysis carried out on several crystals of the sample at $x = 0.5$, previously heated to 1050 °C, showed a Ag/Sb (atom %) ratio of 0.43, which is significantly higher than that determined in the silver antimonate formed at 700 °C (Ag/Sb = 0.24). This fact points to a sublimation of antimony, likely as an antimony oxide. When the sample at $x = 0.5$ was heated to 1035 °C in a closed sample holder, the X-ray pattern showed, in addition to the peaks of the silver antimonate, new peaks of β-Sb_2O_4 (JCPDS 11-0694 file). When the sample at $x = 1.5$ was heated to 1190 °C in an open container, the X-ray diffraction pattern of the residue showed the characteristic peaks of metallic silver (JCPDS 4-0783 file). This result is in agreement with that reported recently on thermally treated $AgSbO_3$.[22] Therefore, our silver antimonates decompose above 950 °C giving a mixture of β-Sb_2O_4, which sublimates, plus metallic silver.

Acknowledgment. The Brazilian−Spanish cooperation project financed by the Agencia Española de Cooperación Internacional (Spanish Ministry of External Affairs) is gratefully acknowledged. We thank Drs. D. M. Nevskaya and M. L. Rojas for mass spectrometry analysis. J.M.A. thanks the Spanish Education and Culture Ministry for a contract under the project MAT 95-0899 (CICYT).

CM9803915